We are IntechOpen, the world's leading publisher of Open Access books Built by scientists, for scientists

6,900
Open access books available

185,000
International authors and editors

200M
Downloads

154
Countries delivered to

Our authors are among the

TOP 1%
most cited scientists

12.2%
Contributors from top 500 universities

CLARIVATE ANALYTICS
BOOK CITATION INDEX
INDEXED

WEB OF SCIENCE™

Selection of our books indexed in the Book Citation Index
in Web of Science™ Core Collection (BKCI)

Interested in publishing with us?
Contact book.department@intechopen.com

Left Ventricular Assist Devices: Engineering Design Considerations

Marwan A. Simaan[1], George Faragallah[1], Yu Wang[1] and Eduardo Divo[2]
[1]University of Central Florida, Orlando, Florida,
[2]Daytona State College, Daytona Beach, Florida,
USA

1. Introduction

Patients with end-stage congestive heart failure awaiting heart transplantation often wait long periods of time (300 days or more on the average) before a suitable donor heart becomes available. The medical community has placed increased emphasis on the use of Left Ventricular Assist Devices or LVADs that can substitute for, or enhance, the function of the natural heart while the patient is waiting for the heart transplant (Poirier, 1997; Frazier & Myers, 1999). Essentially, a rotary LVAD is a pump that operates continuously directing blood from the left ventricle into the aorta by avoiding the aortic valve. Generally speaking, the goal of the LVAD is to assist the native heart in pumping blood through the circulatory system so as to provide the patient with as close to a normal lifestyle as possible until a donor heart becomes available or, in some cases, until the patient's heart recovers. In many situations, this means allowing the patient to return home and/or to the workforce.

The amount of blood pumped by the LVAD into the circulatory system depends on many factors, the most important of which is the rotational speed of the pump which is directly controlled by the pump motor current. The higher the speed of the pump the more blood is forced into the circulatory system. Because of this, an important engineering challenge facing the increased use of these LVADs is the development of an appropriate controller for the speed of the rotor. Such a controller, in addition to being robust and reliable, must satisfy two important criteria:

1. It must be able to adapt to the daily activities and physiological and emotional changes of the patient by regulating the pump speed in order to meet the body's requirements for cardiac output (CO) and mean arterial pressure (MAP) (Olsen, 2000; Boston et al., 2003; Schima et al., 1992; Marieb, 1994).

2. It should ensure that the rotational speed does not exceed an upper limit beyond which the pump will be attempting to draw more blood from the ventricle than available. The occurrence of this phenomenon, known as suction, for a brief period of time may cause collapse of the ventricle resulting in damage to the heart muscle (Yuhki et al. 1999; Vollkron et al., 2006; Ferreira et al., 2006). Suction, therefore, must be detected quickly and the pump speed reduced before any damage to the heart muscle occurs.

The eventual goal of an LVAD speed controller is therefore to meet the above two requirements so that an LVAD recipient patient could potentially leave the hospital and return home to a safe and normal lifestyle. Given that the pump is continuously interacting

with the left ventricle and circulatory system, the development of a speed controller must therefore be done using engineering tools that require a mathematical model of the entire system. The model must be simple enough to be tractable and yet it must be comprehensive enough to capture the essential relationships between the hemodynamic variables and their interactions with the LVAD without the ambiguity of including unnecessary state variables. In this chapter, we discuss the development of such a model. We will first review an autonomous 5th order model of the cardiovascular system, which emphasizes the pressure-volume relationship of the left ventricle. We then present a 1st order model of a rotary LVAD along with its inflow and outflow cannulae and with the pump motor current as its control variable. This model is a variation from the model described in (Simaan et al.; 2009; Simaan, 2009) where the rotational speed was assumed to be the control variable. In reality, the only way the speed can be varied is by varying the pump motor current through a very complex relationship. We account for the phenomenon of suction by adding a nonlinear resistance to the inflow cannula model which becomes active when the left ventricular pressure drops below a certain threshold. Finally, we combine these two models into a 6th order time varying nonlinear model with the pump motor current being the only control variable. The time variations in this model are due to the cyclical nature of the ventricle elastance and its changes as a function of time within one cardiac cycle. The nonlinearities are due to the mitral and aortic valves in the cardiovascular model and the suction resistance in the LVAD model. The binary state of each of these valves yields four consecutive phases within one cardiac cycle during which the ventricle contracts, ejects, relaxes and then fills depending on which valve is open and which is closed. As a result, the mathematical description of the entire model changes as the ventricle crosses from one phase to the next. We will conclude this chapter by outlining some of the challenges in the development of both a feedback speed controller and a suction detection algorithm that need to be overcome before the ultimate goal of the LVAD becomes a reality as well as a discussion of a new Computational Fluid Dynamics (CFD) model of the aortic arch and a Lagrangian particle-tracking model to predict the path of thrombi of different sizes and initial locations traveling across the cardiovascular system. Preliminary results described in this chapter indicate that alignment of the LVAD outflow cannula at different angles of incidence as well as implantation of aortic-to-innominate bypass or aortic-to-left-carotid bypass significantly alters thrombo-embolism rates.

2. The left ventricle circulatory system model

The heart is a very complex system that is very difficult to model mathematically. In research that involves engineering considerations, the development of a mathematical model for the heart is crucial. The model should be complex enough to reproduce the performance of the heart, yet it should be also simple for the computation purposes. For these reasons, we will start, in this section, with a basic model that will be used in the development of feedback controller and suction detection algorithms. Later in the chapter, we will introduce a more complex multi degree-of-freedom (DOF) model that is used in the computational fluid dynamics analysis for prevention of trombo-embolism events.

The basis model assumes that the right ventricle and pulmonary circulation are healthy and normal and as a result their effect on the LVAD can be neglected. A 5th order lumped parameter electric circuit model which can reproduce the left ventricle hemodynamics of the heart (Simaan et al., 2009) is shown in Figure 1. In this model, the behavior of the left
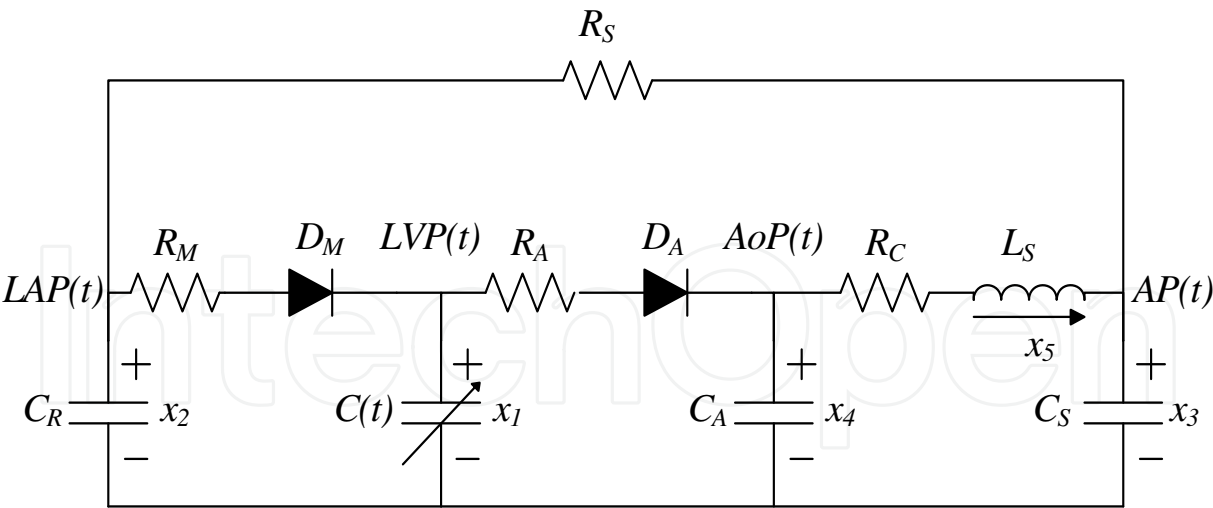
Fig. 1. Cardiovascular electric circuit model

ventricle is modeled by means of a time varying capacitance (or compliance) C(t), which is the reciprocal of the ventricle's elastance function E(t). The elastance represents the contractual state of the left ventricle. It relates to the ventricle's pressure and volume (Suga and Sagawa, 1974) according to the expression:

$$E(t) = \frac{LVP(t)}{LVV(t) - V_0} \qquad (1)$$

where LVP(t) is the left ventricular pressure, LVV(t) is the left ventricular volume, and V_0 is a reference volume, which corresponds to the theoretical volume in the ventricle at zero pressure. The elastance function E(t) can be approximated mathematically. In our work we use the expression:

$$E_H(t) = (E_{max} - E_{min})E_n(t_n) + E_{min} \qquad (2)$$

where $E_H(t)$ represents the elastance of a healthy heart, $E_n(t_n)$ is the normalized elastance (also called "double hill" function) represented by the expression (Stergiopoulos et al., 1996a):

$$E_n(t_n) = 1.55 \cdot \left[\frac{\left(\frac{t_n}{0.7}\right)^{1.9}}{1 + \left(\frac{t_n}{0.7}\right)^{1.9}} \right] \cdot \left[\frac{1}{1 + \left(\frac{t_n}{1.17}\right)^{21.9}} \right] \qquad (3)$$

In the above expression, $E_n(t_n)$ is the normalized elastance, $t_n = t/T_{max}$, $T_{max} = 0.2 + 0.15 t_c$ and t_c is the cardiac cycle interval, i.e., $t_c = 60/HR$, where HR is the heart-rate. Notice that $E_H(t)$ is a re-scaled version of $E_n(t_n)$ and the constants E_{max} and E_{min} are related to the end-systolic pressure volume relationship (ESPVR) and the end-diastolic pressure volume relationship (EDPVR) respectively. Figure 2 shows a plot of $E_H(t)$ for a healthy heart with $E_{max} = 2$ mmHg/ml and $E_{min} = 0.06$ mmHg/ml, and a heart-rate of 60 beats per minute (bpm). For a heart with cardiovascular disease, the elastance expression used in our model is modified

according to $E(t)=\delta E_H(t)$. That is, the elastance $E(t)$ is scaled version of $E_H(t)$ with a factor $0<\delta\leq1$ where $\delta=1$ represents a healthy heart and smaller values of δ are used to represent cardiovascular disease. The more severe the disease is, the smaller the value of δ. Also in the model preload and pulmonary circulations are represented by the capacitance C_R; the aortic compliance is represented by the capacitance C_A, and afterload is represented by the four-element Windkessel model (Stergiopoulos et al., 1996b) comprising R_C, L_S, C_S and R_S. Preload, or venous blood returning to the heart, is closely related to the cardiac output (CO) produced by the heart for a given level of contractility. Afterload can be described as the pressure that the left ventricle has to generate in order to eject blood. It refers to the vascular resistance that the heart sees as it pumps blood. The mitral and aortic valves are represented by two non-ideal diodes consisting of a resistance R_M and ideal diode D_M for the mitral valve, and resistance R_A and ideal diode D_A for the aortic valve. In this representation, we have kept the number of model parameters at a minimum while maintaining enough complexity in the model so that it can reproduce the hemodynamics of the left ventricle. Table 1 lists the various system parameters and their typical associated values (Yu et al. 1998).
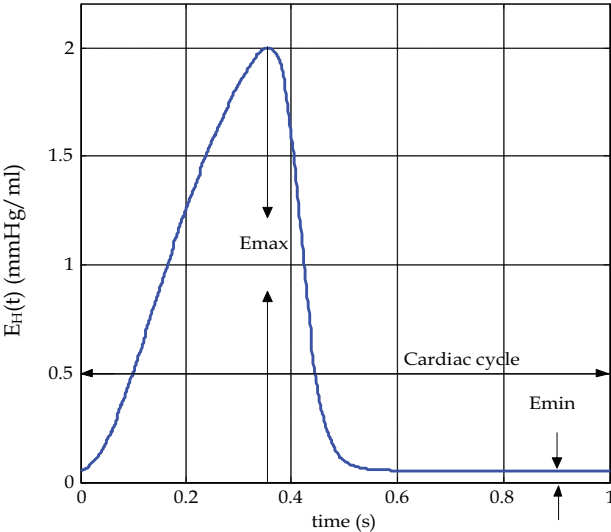

Fig. 2. Elastance function $E(t)=1/C(t)$ of a healthy heart. (Cardiac Cycle =60/HR)

Obviously the circuit model in Figure 1 is time-varying because of the time dependence in $C(t)$ and nonlinear because of the two diodes. Since each diode has two states: open-circuit (o/c) and short-circuit (s/c), four different circuits representing the four different phases of the ventricular functions can therefore be modeled. When the mitral valve is open and aortic valve is closed (i.e. D_M is s/c and D_A is o/c) the circuit in Figure 1 represents the phase when the left ventricle is filling. When the mitral valve is closed and the aortic valve is open (i.e. D_M is o/c and D_A is s/c) the circuit represents the phase when the ventricle is ejecting. When both the mitral and aortic valves are closed (i.e. D_M and D_A are o/c), which occurs twice, the circuit represents the two phases when the ventricle is undergoing isovolumic contraction and relaxation. Finally, the phase when both the mitral and aortic valves are open (i.e. both diodes are s/c) is clearly not feasible. The three different phases of operation of the left ventricle within the cardiac cycle are summarized in Table 2. Every phase is therefore modeled by a different equivalent circuit and hence a different set of linear time-varying differential equations. Instead of writing three different sets of differential

equations, by appropriately modeling the diodes as nonlinear elements, it is possible to write only one set of equations, which describes the behavior of the entire model for all three phases. Selecting the state variables as the hemodynamic variables listed in Table 3 (and shown on the circuit in Figure 1), and using basic circuit analysis techniques (Dorf & Svoboda, 2006) such as Kirchhoff's Voltage and Current Laws (KVL and KCL) we can derive the state equations for the cardiovascular circuit model shown in Figure 1 as follows:

Parameters	Value	Physiological Meaning
Resistances (mmHg·s/ml)		
R_S	1.0000	Systemic Vascular Resistance (SVR)
R_M	0.0050	Mitral Valve Resistance
R_A	0.0010	Aortic Valve Resistance
R_C	0.0398	Characteristic Resistance
Compliances (ml/mmHg)		
$C(t)$	Time-varying	Left Ventricular Compliance
C_R	4.4000	Left Atrial Compliance
C_S	1.3300	Systemic Compliance
C_A	0.0800	Aortic Compliance
Inertances (mmHg·s²/ml)		
L_S	0.0005	Inertance of blood in Aorta
Valves		
D_M		Mitral Valve
D_A		Aortic Valve

Table 1. Model parameters

Modes	Valves		Phases
	Mitral	Aortic	
1	Closed	Closed	Isovolumic Relaxation
2	Open	Closed	Filling
1	Closed	Closed	Isovolumic Contraction
3	Closed	Open	Ejection
-	Open	Open	Not feasible

Table 2. Ventricular phases within one cardiac cycle

Variables	Name	Physiological Meaning (units)
$x_1(t)$	LVP(t)	Left Ventricular Pressure (mmHg)
$x_2(t)$	LAP(t)	Left Atrial Pressure (mmHg)
$x_3(t)$	AP(t)	Arterial Pressure (mmHg)
$x_4(t)$	AoP(t)	Aortic Pressure (mmHg)
$x_5(t)$	$Q_T(t)$	Total flow (ml/s)

Table 3. State variables in the left ventricle circulatory model

$$
\begin{bmatrix} \dot{x}_1 \\ \dot{x}_2 \\ \dot{x}_3 \\ \dot{x}_4 \\ \dot{x}_5 \end{bmatrix} = \begin{bmatrix} \dfrac{-\dot{C}(t)}{C(t)} & 0 & 0 & 0 & 0 \\ 0 & \dfrac{-1}{R_S C_R} & \dfrac{1}{R_S C_R} & 0 & 0 \\ 0 & \dfrac{1}{R_S C_S} & \dfrac{-1}{R_S C_S} & 0 & \dfrac{1}{C_S} \\ 0 & 0 & 0 & 0 & \dfrac{-1}{C_A} \\ 0 & 0 & \dfrac{-1}{L_S} & \dfrac{1}{L_S} & \dfrac{-R_C}{L_S} \end{bmatrix} \begin{bmatrix} x_1 \\ x_2 \\ x_3 \\ x_4 \\ x_5 \end{bmatrix} + \begin{bmatrix} \dfrac{1}{C(t)} & \dfrac{-1}{C(t)} \\ \dfrac{-1}{C_R} & 0 \\ 0 & 0 \\ 0 & \dfrac{1}{C_A} \\ 0 & 0 \end{bmatrix} \begin{bmatrix} \dfrac{1}{R_M} r(x_2 - x_1) \\ \dfrac{1}{R_A} r(x_1 - x_4) \end{bmatrix} \tag{4}
$$

In the above expression $r(\xi)$ represents the ramp function:

$$
r(\xi) = \begin{cases} \xi & \text{if} & \xi \geq 0 \\ 0 & \text{if} & \xi < 0 \end{cases} \tag{5}
$$

We note that the model described above is an autonomous system that does not have an input variable. Validation of this system can be found in (Simaan et al., 2009).

3. The LVAD pump motor current model

The LVAD considered in this paper is a rotary mechanical pump connected with two cannulae between the left ventricle and the aorta. The LVAD pumps blood continuously from the left ventricle into the aorta. The pressure difference between the left ventricle and the aorta is characterized by the following relationship:

$$
LVP(t) - AoP(t) = R_i Q + L_i \frac{dQ}{dt} + R_o Q + L_o \frac{dQ}{dt} + R_p Q + L_p \frac{dQ}{dt} - H_p + R_{su} Q \tag{6}
$$

In the above expression, H_p is the pressure (head) gain across the pump and Q is the blood flow rate through the pump. The parameters, R_i, R_o, and R_p represent the flow resistances and L_i, L_o, and L_p represent the flow inertances of the cannulae and pump respectively. Values for these parameters are shown in Table 4.

Parameters	Value	Physiological Meaning
Cannulae Resistances (mmHg·s/ml)		
R_i	0.0677	Inlet Cannula Resistance
R_p	0.17070	Pump Resistance
R_o	0.0677	Outflow Cannula Resistance
Cannulae Inertances (mmHg·s²/ml)		
L_i	0.0127	Inlet Cannula Inertance
L_p	0.02177	Pump Inertance
L_o	0.0127	Outflow Cannula Inertance

Table 4. Parameter values in LVAD model

The nonlinear time-varying resistance R_{su} in (6) has the form:

$$R_{su} = \begin{cases} 0 & \text{if} \quad LVP(t) > \overline{x}_1 \\ \alpha(LVP(t)-\overline{x}_1) & \text{if} \quad LVP(t) \leq \overline{x}_1 \end{cases} \tag{7}$$

It is included in the model to characterize the phenomenon of suction. Clearly, R_{su} is zero when the pump is operating normally and is activated when $LVP(t)$ (x_1) becomes less than a predetermined small threshold $\overline{x}_1$, a condition that represents suction. The value of R_{su} when suction occurs increases linearly as a function of the difference between $LVP(t)$ and $\overline{x}_1$. The parameter α is a cannula dependent scaling factor. The values used for the suction parameters are $\alpha = -3.5$ s/ml and $\overline{x}_1 = 1$ mmHg.

The pressure gain across the pump H_p is modeled using the direct relation between the electric power supplied to the pump motor P_e and the hydrodynamic power generated by the pump P_p scaled by the pump efficiency η as $P_p = \eta P_e$. Furthermore, the electric power may be written in terms of the supplied voltage V and the supplied current $i(t)$ to the pump motor as $P_e = Vi(t)$, while the hydrodynamic power may be written in terms of the pump head or pressure gain H_p and the pump flow Q as $P_p = \rho g H_p Q$, (Faragallah et al, 2011) where ρ is the density of the reference fluid and g is the acceleration of gravity ($\rho_{Hg} = 13,600$ kg/m³, g=9.8 m/s²). Combining these expressions yields:

$$H_p = \frac{\eta V}{\rho g} \cdot \frac{i(t)}{Q} \tag{8}$$

or,

$$H_p = \gamma \frac{i(t)}{Q} \tag{9}$$

where $\gamma = \eta V/\rho g$. For a typical LVAD, after applying the appropriate conversion factors and assuming a pump motor supplied voltage V=12 volts as well as a pump efficiency of 100% (assuming that most losses are accounted for by the pressure losses induced by R_p and L_p), the constant γ can be computed to be $\gamma = 89,944$ mmHg·ml/s·amp.

Substituting (9) in (6) we obtain the nonlinear state equation governing the behavior of the LVAD as:

$$LVP(t) - AoP(t) = R^*Q + L^* \frac{dQ}{dt} - \gamma \frac{i(t)}{Q} \tag{10}$$

where $R^* = R_i + R_o + R_p + R_{su}$ and $L^* = L_i + L_o + L_p$. Note that it is important to validate the numerical solution when expression (10) is used by ensuring that the system does not allow for operation at zero pump flow $Q(t)$ at any point during the cardiac cycle since equation (10) exhibits its nonlinearity with the pump flow $Q(t)$ in the denominator. Using the relation between the pump pressure H_p and the pump speed $\omega(t)$ (Simaan et al., 2009)) $H_p = \beta\omega^2(t)$, an expression for the pump speed in terms of the pump motor current can be derived as follows:

$$\omega(t) = \sqrt{\frac{\gamma i(t)}{\beta Q(t)}} \tag{11}$$

where $\beta = 9.9025 \cdot 10^{-7}$ mmHg/(rpm)^2. Note that it is now clear how the heart hemodynamics through $Q(t)$ influence directly, in a highly nonlinear manner, the pump speed $\omega(t)$.

4. The combined model with pump motor current as the control variable

The addition of the LVAD to the left ventricle model in (4) will yield the 6th order system shown in Figure 3 and described by the differential equations:

$$
\begin{bmatrix} \dot{x}_1 \\ \dot{x}_2 \\ \dot{x}_3 \\ \dot{x}_4 \\ \dot{x}_5 \\ \dot{x}_6 \end{bmatrix} = \begin{bmatrix} \dfrac{-\dot{C}(t)}{C(t)} & 0 & 0 & 0 & 0 & \dfrac{-1}{C(t)} \\[2mm] 0 & \dfrac{-1}{R_S C_R} & \dfrac{1}{R_S C_R} & 0 & 0 & 0 \\[2mm] 0 & \dfrac{1}{R_S C_S} & \dfrac{-1}{R_S C_S} & 0 & \dfrac{1}{C_S} & 0 \\[2mm] 0 & 0 & 0 & 0 & \dfrac{-1}{C_A} & \dfrac{1}{C_A} \\[2mm] 0 & 0 & \dfrac{-1}{L_S} & \dfrac{1}{L_S} & \dfrac{-R_C}{L_S} & 0 \\[2mm] \dfrac{1}{L^*} & 0 & 0 & \dfrac{-1}{L^*} & 0 & \dfrac{-R^*}{L^*} \end{bmatrix} \begin{bmatrix} x_1 \\ x_2 \\ x_3 \\ x_4 \\ x_5 \\ x_6 \end{bmatrix} + \begin{bmatrix} \dfrac{1}{C(t)} & \dfrac{-1}{C(t)} \\[2mm] \dfrac{-1}{C_R} & 0 \\[2mm] 0 & 0 \\[2mm] 0 & \dfrac{1}{C_A} \\[2mm] 0 & 0 \\[2mm] 0 & 0 \end{bmatrix} \begin{bmatrix} \dfrac{1}{R_M} r(x_2 - x_1) \\[2mm] \dfrac{1}{R_A} r(x_1 - x_4) \end{bmatrix} + \begin{bmatrix} 0 \\ 0 \\ 0 \\ 0 \\ 0 \\ \dfrac{\gamma}{L^*} x_6 \end{bmatrix} i(t) \quad (12)
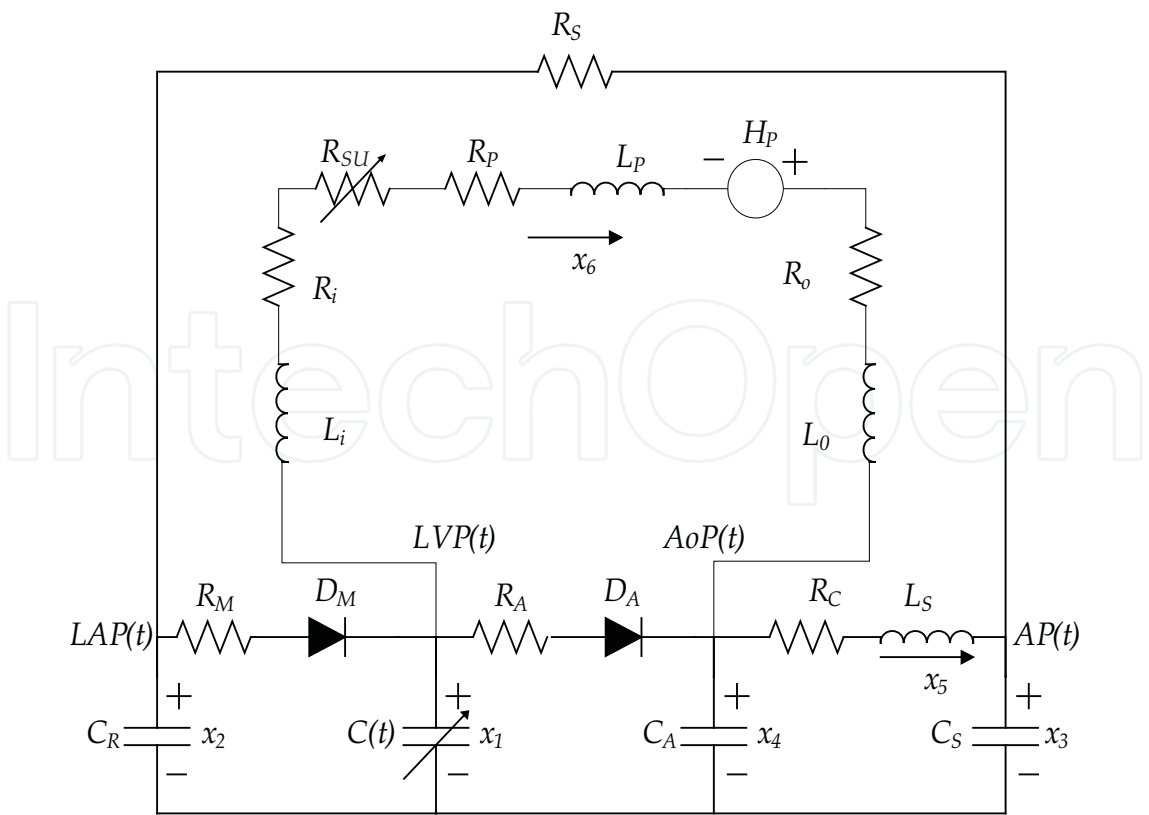$$

Fig. 3. Combined cardiovascular and LVAD model

Note that the additional state variable $x_6(t) = Q(t)$ represents the blood flow through the pump. Eight other passive variables: R_i, R_p, R_o, R_{su}, L_i, L_p, L_o (see Table 4) and a parameter γ have also been added. The combined model (12) is now a forced system where the control variable is the supplied current to the pump motor i(t).

Note that one of the state variables, specifically $x_6(t)$, appears in the denominator of the right-hand side of the system in (12). Therefore, special care must be taken in the numerical solution of the system as the non-linearity can significantly affect the stability of the solution algorithm. In this case, a simple time-lagging combined with a sub-level iteration scheme was devised to control the stability of the numerical solution process.

5. Considerations in the development of a feedback controller

Clearly the model derived above allows for the LVAD to be controlled by its pump motor i(t) instead of its pump speed $\omega(t)$. In this model i(t) must be adjusted to meet the patient needs for cardiac output while at the same time keeping the speed in the safe region to avoid suction. Since until very recently, most LVAD models have used the pump speed as the control variable, it is important at this stage to validate the model by examining how the pump speed is affected when using the pump motor current i(t) as the control variable.
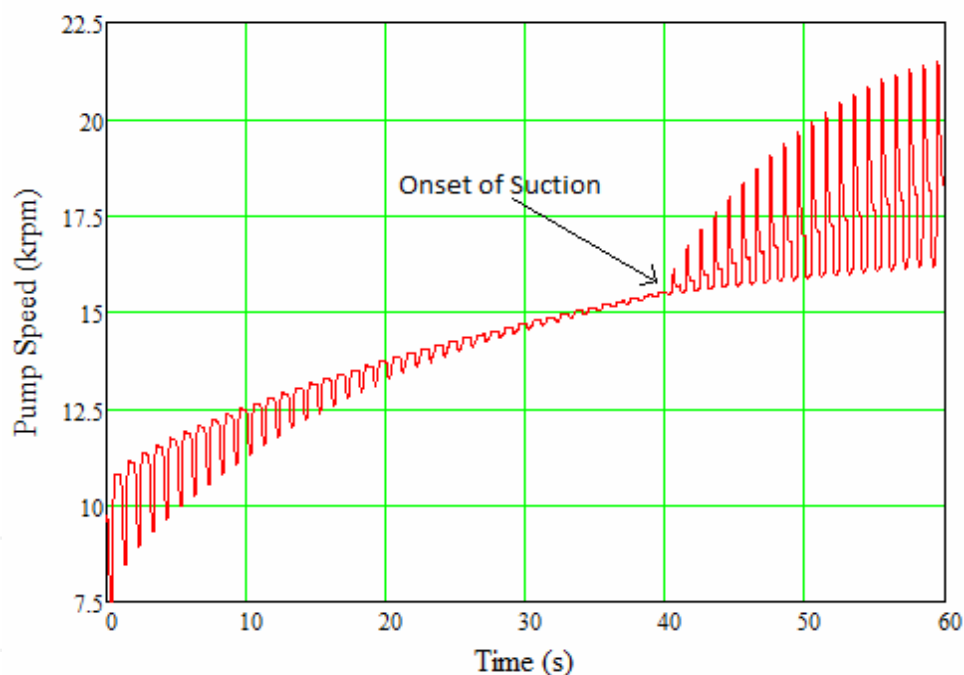

Fig. 4. Pump speed signal as a function of time derived from our model when the pump motor current is increased linearly

Figure 4 shows a plot of the pump speed when the model, with a heart rate HR=60 bpm, is excited with a linearly increasing pump current starting at i(0)=0.1 amp and increasing with a slope m=0.01 amp/s. There are several important observations that can be made from this figure. First, note that the resulting pump speed $\omega(t)$ does not also increase linearly. Instead, it increases nonlinearly with a decreasing rate of increase. Second, the pump speed has a superposed oscillatory component that has the same pulsatility as HR. This is a very interesting and an extremely important new phenomenon that has recently been observed in

in-vivo data obtained through clinical studies of intensive care patients implanted with LVADs (Mason et al. 2008). This is the first time that such a phenomenon has been reproduced from a combined cardiovascular and LVAD model and represents a breakthrough in accurately modeling this complex bio-mechanical system.

A third observation that can be made from Figure 4 is that the amplitude of the oscillatory component in the pump speed signal ω(t) seems to decrease in time up to a point when a breakdown occurs and the amplitude exhibits a sudden increase when the pump current is increased beyond this point. In Figure 4 this breakdown occurs at t=40 s which corresponds to a pump speed of 15,500 rpm. Clearly this value of pump speed corresponds to the onset of suction as will be discussed in the next section.

6. Considerations in the development of suction detection algorithm

An important constraint that should be taken into consideration in designing any LVAD controller is to ensure that the pump is rotated at a speed below a threshold beyond which the pump will attempt to draw more blood from the left ventricle than available causing a phenomenon called ventricular suction. This phenomenon, which could cause collapse of the ventricle, is dangerous and needs to be detected and corrected immediately by decreasing the pump motor current, hence lowering the pump speed below the suction threshold.

Several approaches have been used to detect suction. Among these are ones that extract features from the pump flow signal. This signal is one of very few signals that can be easily measured. These approaches use powerful pattern recognition algorithms to classify the signal into being in or out of suction. These classifiers vary from simple threshold comparisons (Oshikawa et al., 2000) to more complex techniques such as Classification and Regression Tree (CART) (Karantonis et al., 2006), Discriminant Analysis (DA) (Ferreira et al., 2006), and Neural Networks (NN) (Karantonis et al., 2008).

In this chapter, we describe a new suction detection and classification algorithm based on the Lagrangian Support Vector Machine (LSVM) method in pattern recognition (Wang et al., 2011). The LSVM is a modified version of the standard Support Vector Machine (SVM) and is characterized by high accuracy, stable performance, and fast learning speed. Several real-time applications of the SVM method in different fields have been reported in the literature (Sitaram et al., 2011; Gabran et al., 2009).

Figure 5 shows the flow chart of the proposed algorithm. The feature extraction module calculates several indices from the processed pump flow. These indices then allow a determination of the pump status as one of three states separated by two threshold values on the quantity:

$$\Delta P = MLVP\text{-}MPIP$$

where MLVP is the Minimum Left Ventricular Pressure and MPIP is the Minimum Pump Inlet Pressure. The low threshold ΔP_{NS} is the No Suction threshold and the high threshold ΔP_S is the Suction threshold. The three states of the pump status are:

1. *No Suction (NS):* This corresponds to the normal operating condition of the pump. This state is characterized by $\Delta P \leq \Delta P_{NS}$. In this case, the pump flow signal is periodic with a large sinusoidal component.

2. *Approaching Suction (AS):* In this case, $\Delta P_{NS} < \Delta P \leq \Delta P_S$ which means MPIP decreases much faster than MLVP causing ΔP to increase. The pump flow signal becomes less pulsatile compared to the No Suction case.

3. *Suction (S):* In this case $\Delta P > \Delta P_S$. During this event, the inlet cannula is evidently obstructed, MPIP exhibits very large negative spikes, and MLVP is slightly less than zero. The pump flow signal exhibits complex non-periodic behavior with a sudden large drop in the slope of the envelope of the minimum pump flow signal.

Several indices based on time domain, frequency domain, and time-frequency domain can be extracted from the pump flow signal $x_6(t)$ to use in the classifier (Ferreira et al. 2006). In this chapter we describe three possible time-domain indices, SI_1, SI_2 and SI_3, two frequency-domain indices SI_4 and SI_5, and one time-frequency domain index SI_6 for a total of six possible indices that are used by the LSVM classifier.

The first time domain index SI_1 is defined as follows (Vollkron, et al. 2004):

$$SI_1 = \frac{2 \times \text{mean}(x_6(t)) - [\max(x_6(t)) + \min(x_6(t))]}{\max(x_6(t)) - \min(x_6(t))} \tag{13}$$

where mean $(z(t))$, max$(z(t)$ and min$(z(t))$ denote the mean, maximum and minimum values of signal $z(t)$ respectively. When suction is absent, the mean pump flow value is approximately half of the sum of the maximum and minimum values of pump flow, which shifts slightly towards minimum pump flow while approaching suction. When suction occurs, the mean pump flow value is close to the maximum pump flow value. Hence, SI_1 increases dramatically.

Training   **Testing**

Raw Data (Pump Flow)   Raw Data (Pump Flow)

Pre-processing   Pre-processing
- Remove Mean   - Remove Mean
- Pre-filtering   - Pre-filtering

Feature Extraction   Feature Extraction
- Time Domain   - Time Domain
- Frequency Domain   - Frequency Domain
- Time-Frequency Domain   - Time-Frequency Domain

LSVM Classifier Training   Classification

Trained LSVM Classifier   Classifier Performance Evaluation
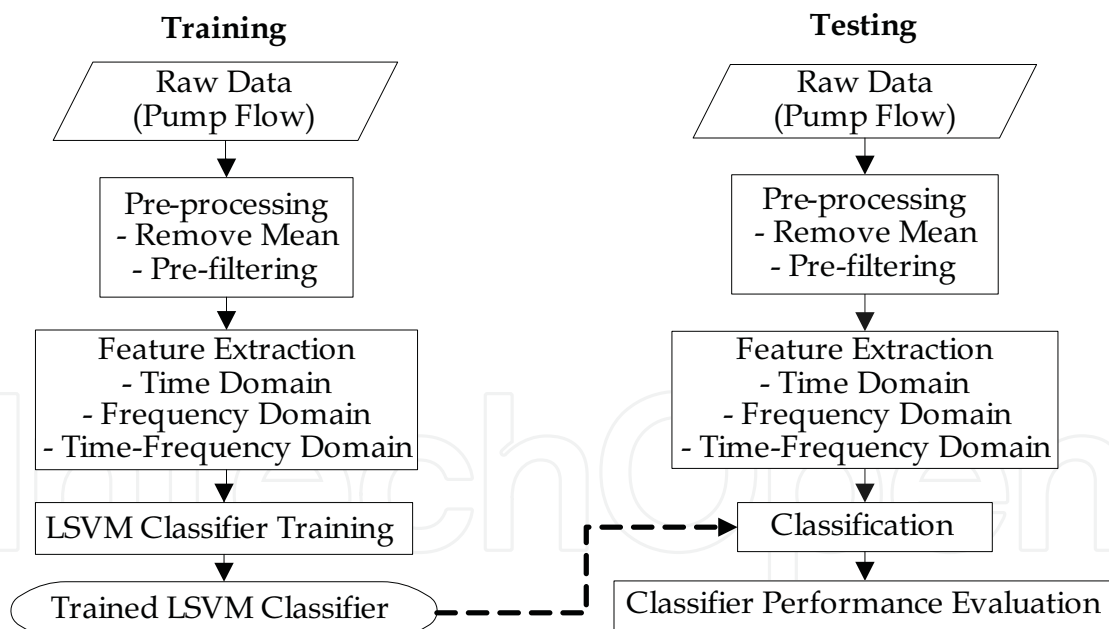
Fig. 5. Flow chart of the proposed suction detection algorithm

The other two indices SI_2 and SI_3 are calculated in terms of the derivative of the pump flow signal $x_6(t)$ as follows:

$$SI_2 = \frac{\max\left[\dfrac{dx_6(t)}{dt}\right]}{\max(x_6(t)) - \min(x_6(t))} \quad \text{and} \quad SI_3 = \frac{\min\left[\dfrac{dx_6(t)}{dt}\right]}{\max(x_6(t)) - \min(x_6(t))} \tag{14}$$

Obviously SI_2 increases during suction, whereas SI_3 decreases at the beginning of suction. The frequency-domain indices SI_4 and SI_5 are calculated as follows (Ferreira et al., 2006):

$$SI_4 = \frac{\int_{\omega_1}^{\omega_2} |Q_P(\omega)| d\omega}{\int_{\omega_2}^{\infty} |Q_P(\omega)| d\omega} \quad \text{and} \quad SI_5 = \frac{\int_0^{\omega_1} |Q_P(\omega)| d\omega}{\int_{\omega_1}^{\omega_2} |Q_P(\omega)| d\omega} \tag{15}$$

where $Q_P(\omega)$ is the Fourier transform of the pump flow signal $x_6(t)$ and ω_0 is the fundamental frequency in this signal, $\omega_1=\omega_0-\omega_c$ and $\omega_2=\omega_0+\omega_c$, where ω_c is a threshold (in radians) that defines an interval centered at ω_0. The index SI_4 is a measure of the ratio of the signal's total energy in the fundamental component frequency band to the total energy in the harmonic component frequency band and SI_5 is a measure of the ratio of the subharmonic energy to the fundamental energy. When approaching suction, SI_4 starts to decrease and SI_5 starts to increase. When suction starts, SI_4 decreases and SI_5 increases abruptly. This is due to the shift of energy from the fundamental band to both the harmonic and subharmonic bands, indicating that suction is taking place.

Finally the time-frequency-domain index SI_6 is defined as the standard deviation of instantaneous mean frequency of the pump flow signal expressed as (Ferreira et al., 2006):

$$SI_6 = \sqrt{var(\langle \omega \rangle_t^{sp})} \tag{16}$$

where the instantaneous frequency is defined as the average frequency at a given time (Cohen, 1995) and expressed as:

$$\langle \omega \rangle_t^{sp} = \frac{\int \omega P_{sp}(\omega,t) d\omega}{\int P_{sp}(\omega,t) d\omega} \tag{17}$$

where $P_{SP}(\omega,t)$ is the squared magnitude of the short-time Fourier transform (STFT). The value of SI_6 is small when suction is not occurring and increases slightly when suction is approaching, and it increases abruptly when suction starts.

We will now illustrate the performance of the LSVM classifier. Figure 6(a) shows a pump flow signal of an LVAD in vivo experiment used in (Ferreira et al., 2006). The six suction indices derived from this signal are also plotted on the same figure. The changes in these indices as the pump flow signal transitions from NS to AS then to S are clearly evident in Figure 6(b)-(g). These indices are used as inputs to the LSVM classifier. The classifier is trained on a randomly selected set of 50% of the data and then tested on the remaining 50% of the data. The two thresholds on ΔP used in the classifier, as mentioned earlier, where chosen as $\Delta P_{NS}=10$ mmHg and $\Delta P_S=35$ mmHg. Due to the random selection of data samples, the classification is repeated 100 times. The average classification results of the proposed algorithm over 100 runs on the test set are shown in Table 5.

	NS	AS	S	Total
NS	703.14	53.36	0.5	757
AS	37.33	598.24	5.43	641
S	0.09	5.31	94.6	100

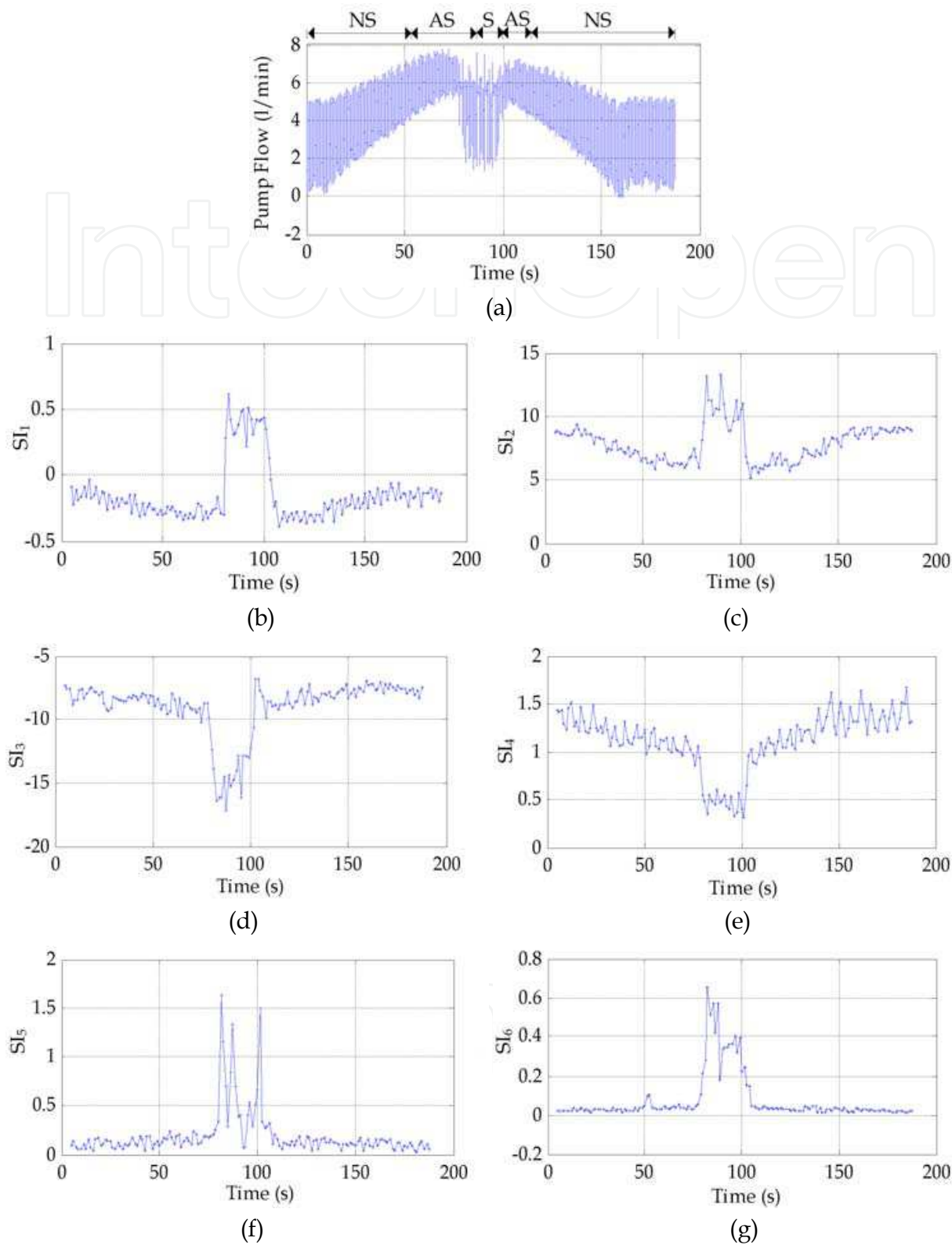Table 5. Classification results of the LSVM Classifier (actual classes are in rows, predicted classes are in columns)

Fig. 6. Suction indices extracted from the pump flow. (a) Pump Flow. (b) SI_1. (c) SI_2. (d) SI_3. (e) SI_4. (f) SI_5. (g) SI_6

For NS, on average there are 53.36 samples misclassified as AS (7.05%) and only 0.5 samples are misclassified as S (0.06%). For AS, on average 37.33 samples are misclassified as NS

(5.82%) and only 5.43 samples are incorrectly identified as S (0.85%). For S, on average the erroneous number of samples misclassified as NS and AS are as low as 0.09 (0.09%) and 5.31 (5.31%), respectively.

7. Considerations in adjustment of angle of incidence in LVAD implantation

Like suction, stroke is another crucial complication that may result due to LVAD therapy. The incidence of such thrombo-embolic cerebral events is reduced by anticoagulation management and improved LVAD design. Still, the incidence of such events is relatively high accounting for about 19% of patients and a mortality rate of 65% (Davies et al., 2008, Russo et al., 2009, Thoennissen et al., 2006, and Schmid et al., 1998). It may be hypothesized that cerebral thrombo-embolism may be reduced by adjusting the placement and angle of incidence of the LVAD outflow cannula as well as by the implantation of an aortic-to-innominate artery bypass or an aortic-to-left-carotid artery bypass. In this section, results are presented of a numerical study conducted based on a multi-scale model where the electric circuit model of the cardiovascular/LVAD circulation as the one previously discussed is used to impose the transient fluid flow boundary conditions at the aortic arch circulation by coupling it with a Computational Fluid Dynamics (CFD) model and a Lagrangian particle-tracking model to predict the path of thrombi of different sizes and initial locations traveling across the cardiovascular system.

In order to properly account for the unsteady nature of the flow field generated by the cardiac ejection in an Aortic Arch with an implanted LVAD a closed-loop external vascular model is necessary. Such external model is coupled to the CFD model to dictate the flow field boundary conditions at the outlets of the CFD model and thus, control the flow splits through the different branches that stem out of the aortic arch throughout the cardiac cycle. To this end, a Multi-DOF (degrees of freedom) electric circuit model representing the different flow and pressure values at the different elements of the external cardiovascular model was constructed as seen in Figure 7.

We utilize the CFD code, STARCCM+, in which a Lagrangian particle-tracking model is coupled to the fluid flow solver to predict particle trajectories. In this study, we then explore the possibility of finding an optimal configuration of the LVAD conduit angle and anastomosis location (that is both distance from the innominate and polar angle in the coronal plane of the ascending aorta), and we seek to establish the benefits of the ligation of the innominate artery and placement of an aortic-to-innominate artery bypass graft or the ligation of the left carotid artery and placement of an aortic-to-left-carotid artery bypass graft.

As a preliminary approach to solve this problem, the LVAD conduit flow is assumed to be steady (non-pulsatile), with negligible pulsatile flow originating from the aortic root. Although not always the case, steady or near steady flow characterizes the flow regime in many patient with LVAD support (Shahcheraghi et al., 2002; Tokuda et al., 2008; and Drummond et al., 2008). Continuous-flow LVADs have predominantly become the device of choice. Consequently, the focus of this study is to investigate steady flow conditions and therefore, steady flow splits are imposed as boundary conditions at the outlet branches of the aortic arch rather than coupling this with the Multi-DOF electric circuit model in Figure 7. Future studies will be conducted taking into account the unsteady behavior of the flow field and the interaction with the external cardiovascular circuit.
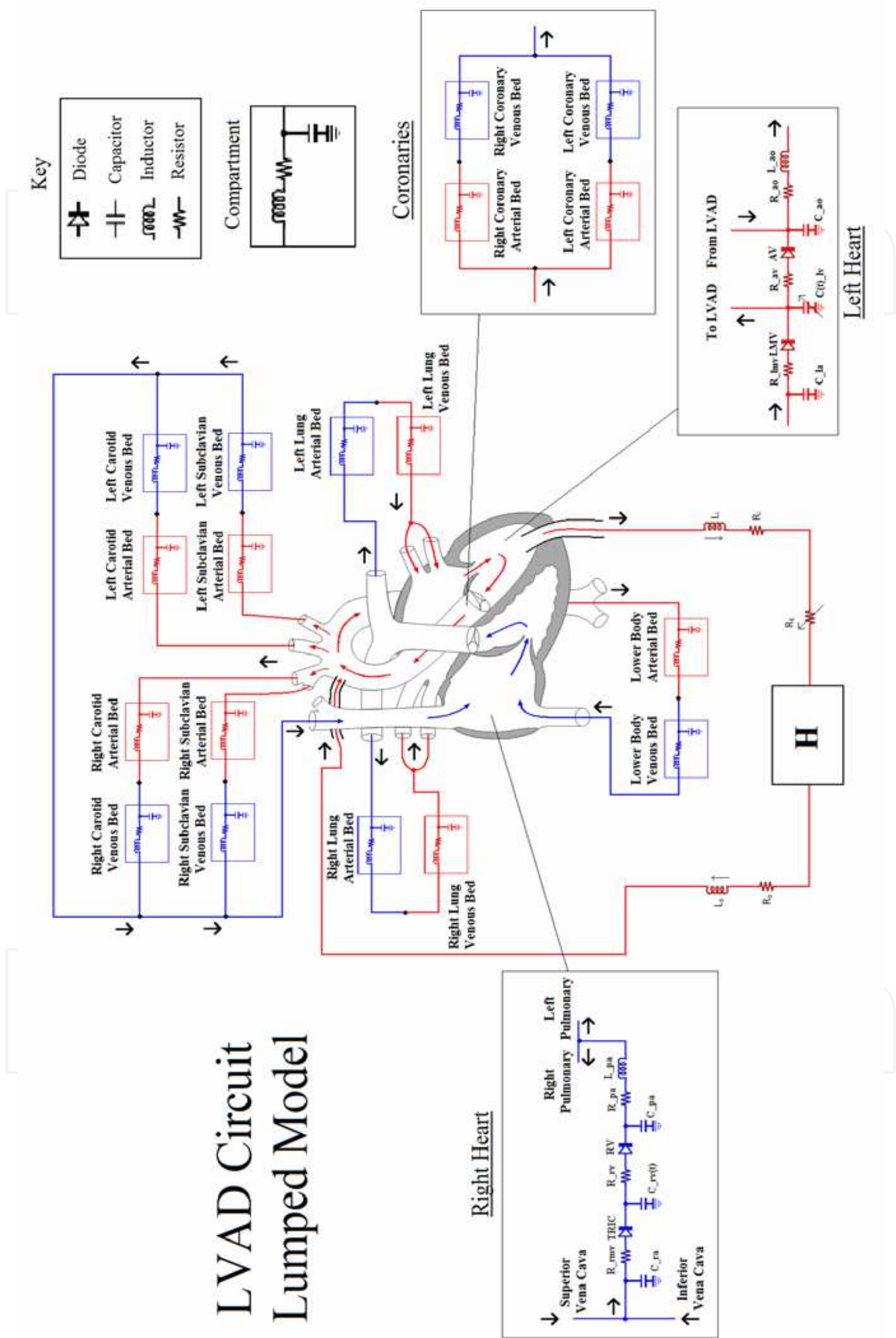
Fig. 7. Multi-DOF electric circuit used to generate the boundary condition waveforms

Figure 8 illustrates the typical geometry of a human aortic arch (Layton et al., 2006) indicating the names of the different branches that stem out of the arch. Figure 9(a)-(c) shows the proposed CFD solid models with the LVAD conduit at (a) normal angle of incidence $\alpha=0°$, (b) intermediate angle of incidence $\alpha=30°$, and shallow angle of incidence $\alpha=60°$. Figure 10(a)-(b) presents the proposed CFD solid models with the LVAD conduit at normal angle of incidence and (a) aortic-to-innominate (IA) bypass and (b) aortic-to-left-carotid (LCA) bypass.
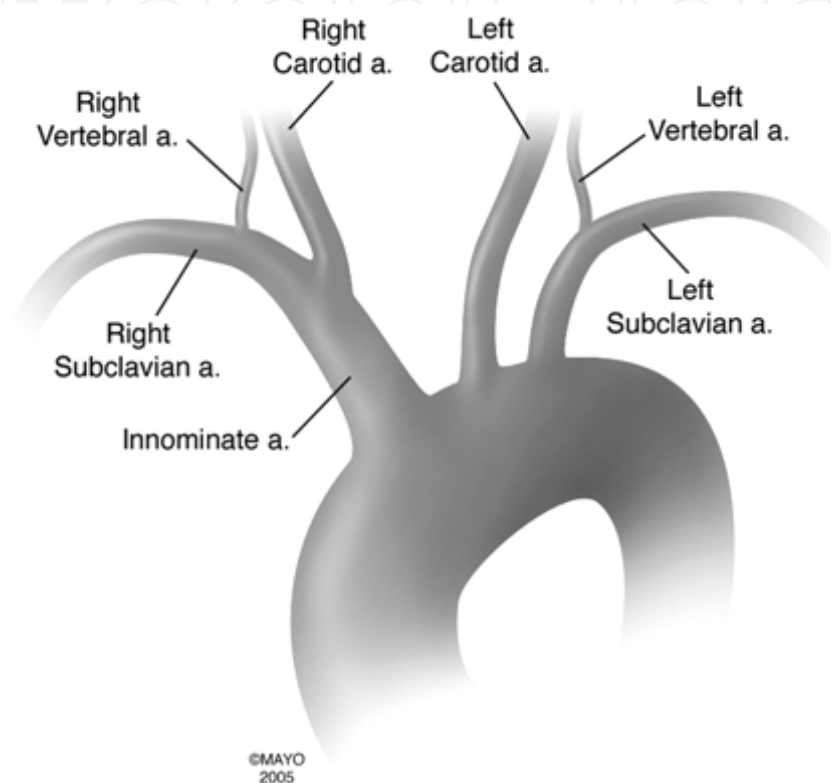
Fig. 8. Most common form of aortic arch in humans (Layton et al., 2006)

Results are presented in the form of velocity vector plots colored by velocity magnitudes around the vicinity of the LVAD cannula anastomosis to the aortic root in Figure 11 (a)-(c) for the different angles of incidence, illustrating the local hemodynamics behavior with pronounced recirculation zones. Table 6 presents the percentage of particle embolization (flow of particles to the left or right Carotid arteries) for the different angles and bypass cases calculated using the particle tracking model by releasing 900 solid, perfectly spherical, particles of diameters 2mm, 4mm and 5 mm, at random locations of the cross-section of the LVAD cannula. These averages reveal significant differences in thrombo-embolization by adjustment of the LVAD inflow cannula and placement of bypass grafts, showing a maximum rate of embolization of close to 50% at shallow angles of incidence in contrast to embolization rates of about 12% at intermediate angles of incidence with bypass implantation. These preliminary results (see Osorio et al., 2009, and El-Zahab et al., 2010) are promising and can potentially offer guidance to surgeons as to the optimal implantation angle and location of the LVAD cannula as well as to the potential implantation of aortic bypass grafts to minimize stroke risk.
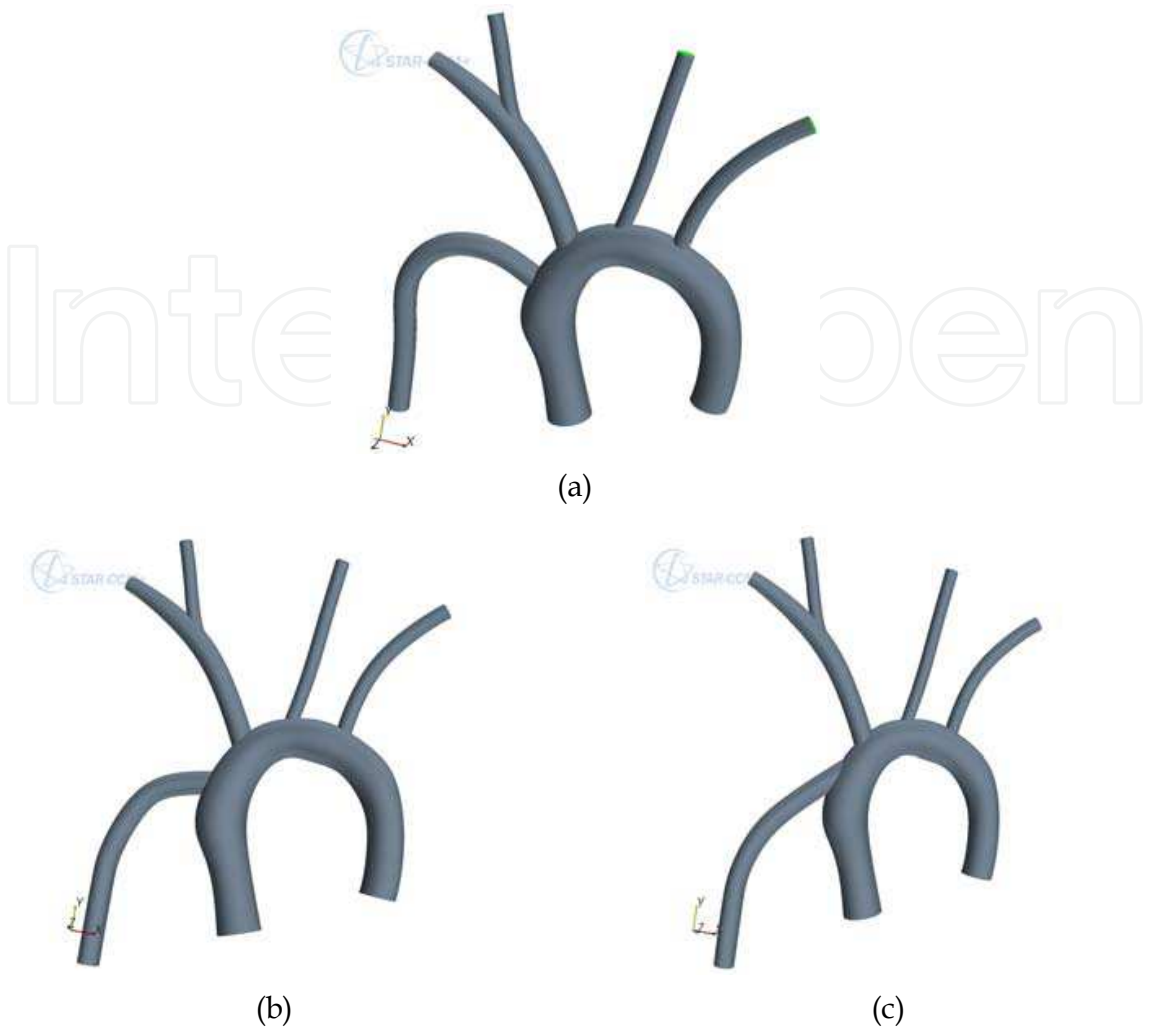
Fig. 9. Solid model of adult aortic arch with LVAD conduit at (a) normal angle of incidence α=0°, (b) intermediate angle of incidence α=30°, and (c) shallow angle of incidence α=60°

Fig. 10. Solid model of adult aortic arch with LVAD conduit at normal angle of incidence and (a) aortic-to-innominate (IA) bypass and (b) aortic-to-left-carotid (LCA) bypass
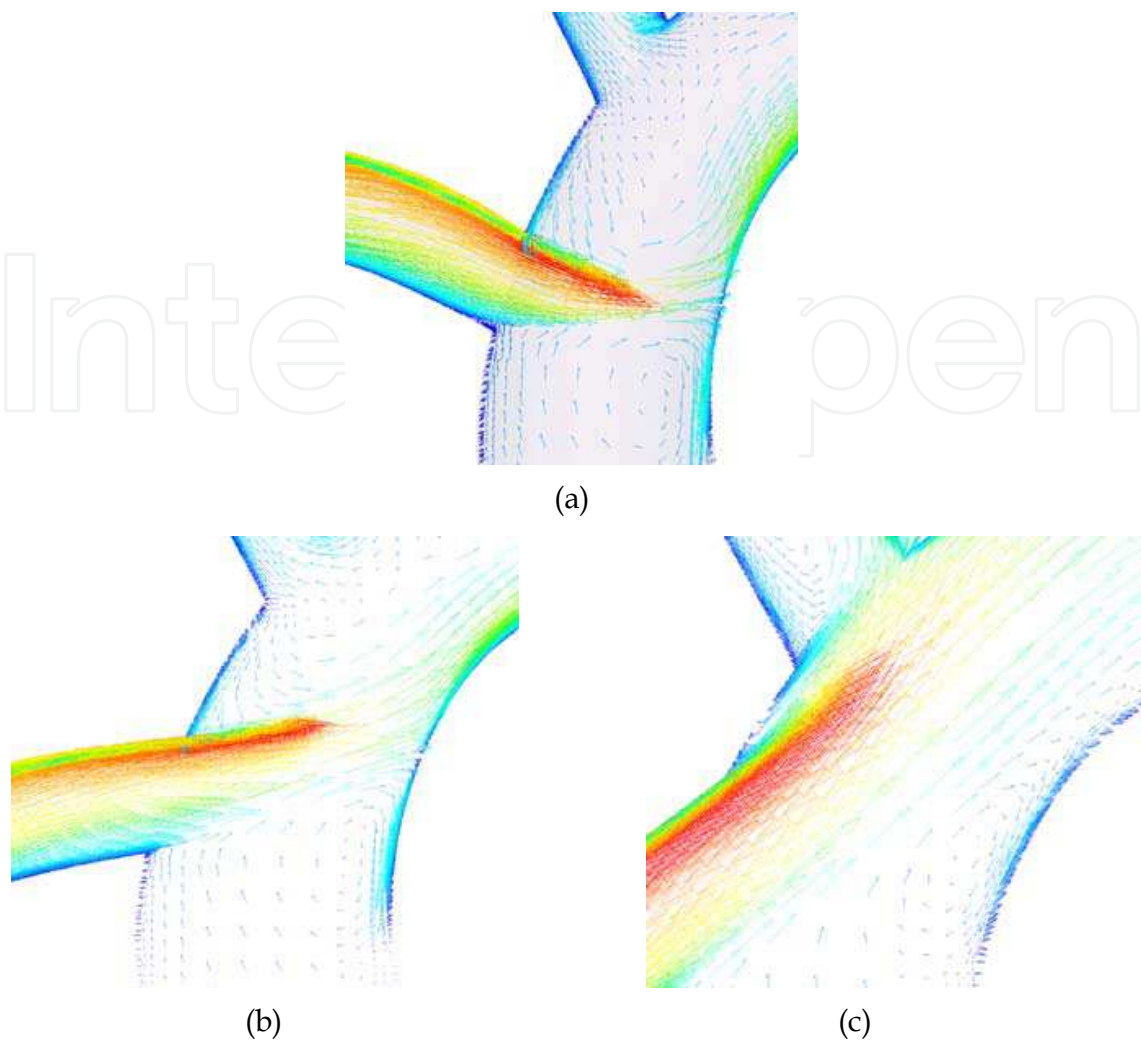
(a)

(b)

(c)

Fig. 11. CFD results in the form of vector plots colored by velocity magnitude for LVAD conduit at (a) normal angle of incidence α=0°, (b) intermediate angle of incidence α=30°, and (c) shallow angle of incidence α=60°

Configuration	Overall [%]
Standard α=0°	25.60±17.06
IA Bypass α=0°	20.54±10.06
LCA Bypass α=0°	40.93±22.34
Standard α=30°	20.57±9.33
IA Bypass α=30°	14.51±7.62
LCA Bypass α=30°	12.72±5.30
Standard α=60°	47.43±6.44
IA Bypass α=60°	55.66±8.31
LCA Bypass α=60°	34.74±25.98

Table 6. Overall percentage of embolization (thrombi flowing to the LCA and RCA) for the different LVAD conduit angle and bypass configurations

8. Conclusion

In this chapter, we discussed some of the engineering considerations and challenges faced in the design and development of a rotary LVAD. In particular, we presented (1) a current based mathematical model that is appropriate for the design of a feedback controller for the LVAD, (2) an effective algorithm for detection of suction in the left ventricle, and (3) a method for alignment of the outflow cannula of an implanted LVAD to minimize the rate of occurrence of patient trombo-embolic cerebral events.

The model we presented in this chapter is dynamic, 6th order and in state-space format. It represents the combined bio-mechanical system of the LVAD connected to a failing left ventricle with a much reduced elasticity function. The control variable in this model is the pump motor current instead of the pump rotational speed, which so far has been the predominant control variable used in the currently existing models. This model is much more useful for the development of an optimal controller for the LVAD since it avoids solving the inverse problem for determining the pump motor current that yields an already determined optimal pump speed protocol. A method for detecting ventricular suction based on six indices determined from the pump flow signal was also developed. This method is based on the well-known Lagrangian Support Vector Machine technique in pattern recognition. Any feedback controller for the LVAD must take into consideration the detection and avoidance of ventricular suction. Finally, results of a numerical study using Computational Fluid Dynamics and a Lagrangian particle tracking model to predict the path of trombi of different sizes and initial location traveling from the outflow cannula into the circulatory system were presented. This study should be very useful in considering the adjustment of the angle of incidence of the outflow cannula to avoid the occurrence of trombo-embolic cerebral events in LVAD patients.

9. Acknowledgements

10. References

Boston, J.; Antaki, J. & Simaan, M. (2003). Hierarchical Control of Hearts Assist Devices. *IEEE Robotics and Automation Magazine,* Vol. 10, No.1, pp. 54-64

Cohen, L. (1995). *Time-Frequency Analysis*. Prentice-Hall, Englewood Cliffs, NJ

Davies, R.; Russo, M.; Hong, K.; O'Byrne, M.; Cork, D.; Moskowitz, A.; Gelijns, A.; Mital, S.; Mosca, R. & Chen, J. (2008). The use of mechanical circulatory support as a bridge to transplantation in pediatric patients: an analysis of the United Network for Organ Sharing database. *The Journal of Thoracic and Cardiovascular Surgery*, Vol. 135, No. 2, pp. 421-427

Dorf, R. & A. Svoboda, J. (2006). *Introduction to Electric Circuits* (7th Edition), John Wiley

Drummond, A.; Onur Dur, O.; Pekkan, K. & Antaki, J. (2008). Simulation of Optimal Surgical Anastomosis of Pediatric Aortic Cannula. *Proceedings of the American Society of Mechanical Engineers Summer Bioengineering Conference (SBC2008),* Paper SBC2008-193064

El-Zahab, Z.; Divo, E. & Kassab, A. (2010). Minimization of the Wall Shear Stress Gradients In Bypass Grafts Anastomoses using Meshless CFD and Genetic Algorithms Optimization. *Computer Methods in Biomechanics and Biomedical Engineering*, Vol. 13, No. 1, pp. 35 – 47

Faragallah, G.; Wang, Y.; Divo, E. & Simaan, M. (2011). A new current-based control model of the combined cardiovascular and rotary left ventricular assist device. *Proceedings of the 2011 American Control Conference*, San Francisco, CA, June 29- July 1, 2011, pp. 4776-4780

Ferreira, A.; Chen, S.; Simaan, M.; Boston, J. & Antaki, J. (2006). A discriminant-analysis-based suction detection system for rotary blood pumps. *Proceedings of 28th IEEE Annual International Conference of Engineering in Medicine and Biology*, New York, NY, 2006, pp. 5382–5385

Frazier, O. & Myers, T.J. (1999) Left Ventricular Assist Systems as a Bridge to Myocardial Recovery. *Annals of Thoracic Surgery*, Vol. 68, pp. 734-741

Gabran, S.; Moussa, W.; Salama, M. & George, C. (2009). Portable real-time support-vector-machine-based automated diagnosis and detection device of narcolepsy episodes. *Proceedings of 31st IEEE Annu. International Conference of Engineering in Medicine and Biology*, Minneapolis, MN, Sep. 2-6, 2009, pp. 903–906

Karantonis, D.; Lovell, N.; Ayre, P.; Mason, D. & Cloherty, S. (2006). Identification and classification of physiologically significant pumping states in an implantable rotary blood pump. *Artificial Organs,* vol. 30, no. 9, pp. 671-679

Karantonis, D.; Cloherty, S.; Lovell, N.; Mason, D.; Salamonsen, R. & Ayre, P. (2008). Noninvasive detection of suction in an implantable rotary blood pump using neural networks. *International Journal of Computation Intelligence and Applications*, vol. 7, pp. 237-247

Layton, K.; Kallmes, D.; Cloft, H.; Lindell, E & Cox, V. (2006). "Bovine Aortic Arch Variant in Humans: Clarification of a Common Misnomer," *American Journal of Neuroradiology*. Vol. 27, pp. 1541-1542

Mason, D.; Hilton, A. & Salamonsen, R. (2008). Reliable Suction Detection for Patients with Rotary Blood Pumps. *The American Society for Artificial Internal Organs (ASAIO) Journal*, Vol. 54, pp. 359-366

Marieb, E. (1994). *Human Anatomy and Physiology*. Pearson Education, San Francisco, CA

Olsen, D. (2000). The History of Continuous-Flow Blood Pumps. *Artificial Organs*, Vol. 24, No. 6, pp. 401-404

Oshikawa, M.; Araki, K.; Endo, G.; Anai, H. & Sato, M. (2000). Sensorless controlling method for a continuous flow left ventricular assist device. *Artificial Organs*, vol. 24, no. 8, pp. 600-605

Osorio, A.; Kassab, A.; Divo, E.; Argueta-Morales, R. & DeCampli, W. (2009). Computational Fluid Dynamics Analysis of Surgical Adjustement of Ventricular Assist Device Implantation to Minimize Stroke Risk, *American Society of Mechanical Engineers,* paper IMECE2009-12813

Poirier, V. (1997). The LVAD: A Case Study. *The Bridge*, Vol. 27, pp. 14-20

Russo, M.; Hong, K.; Davies, R.; Chen, J.; Sorabella, R.; Ascheim, D.; Williams, M.; Gelijns, A.; Stewart, A.; Argenziano, M. & Naka, Y. (2009). Posttransplant survival is not diminished in heart transplant recipients bridged with implantable left ventricular assist devices. *The Journal of Thoracic and Cardiovascular Surgery*, Vol. 138, No. 6, pp.1425-1432

Schmid, C.; Weyand, M.; Nabavi, D.; Hammel, D.; Deng, M.; Ringelstein, E. & Scheld, H. (1998). Cerebral and systemic embolization during left ventricular support with the Novacor N100 device. *The Annals of Thoracic Surgery*, Vol. 65, No. 6, pp.1703-1710

Shahcheraghi, N.; Dwyer, H.; Cheer, A.Y.; Barakat, A.I. & Rutaganira, T. (2002). Unsteady and Three-Dimensional Simulation of Blood Flow in the Human Aortic Arch. *American Society of Mechanical Engineers Journal of Biomechanical Engineering*, Vol. 124, No. 4, pp. 378-387.

Tokuda, Y.; Song, M-H; Ueda, Y.; Usui, A.; Akita, T.; Yoneyama, S. & Maruyama, S. (2008). Three-dimensional numerical simulation of blood flow in the aortic arch during cardiopulmonary bypass. *European Journal of Cardio-thoracic Surgery*, Vol.33, pp. 164-167

Schima, H.; Trubel, W.; Moritz, A.; Wieselthaler, G.; Stohr, H.; Thoma, H.; Losert, U. & Wolner, E. (1992). Noninvasive Monitoring of Rotary Blood Pumps: Necessity, Possibilities, and Limitations. *Artificial Organs*, Vol. 14, No. 2, pp. 195-202

Simaan, M. A.; Ferreira, A.; Chen, S.; Antaki, J. & Galati, D. (2009). A Dynamical State-Space Representation and Performance Analysis of A Feedback-Controlled Rotary Left Ventricular Assist Device. *IEEE Transactions on Control Systems Technology*, Vol.17, No. 1, (January 2009), pp. 15-28

Simaan, M. A. (2009). *Rotary Heart Assist Devices*. Chapter 79 in Springer Handbook of Automation, Nof (ED). pp. 1409-1422

Sitaram, R.; Lee, S.; Ruiz, S.; Rana, M.; Veit, R. & Birbaumer, N. (2011) Real-time support vector classification and feedback of multiple emotional brain states. *Journal of NeuroImage*, Vol. 56, pp. 753-765

Stergiopulos, N.; Meister, J. & Westerhof, N. (1996a). Determinants of Stroke Volume and Systolic and Diastolic Aortic Pressure. *American Journal of Physiology*, Vol. 270, No. 6, 1996, pp. H2050-H2059

Stergiopulos, N.; Westerhof, B.; Meister, J. & Westerhof, N. (1996b). The Four Element Windkessel Model. *Proceedings of the 18th IEEE Engineering in Medicine and Biology Annual International Conference*, Amsterdam, Holland, 1996, pp. 1715-1716

Suga, H. & Sagawa, K. (1974). Instantaneous Pressure-Volume Relationships and Their Ratio in the Excised, Supported Canine Left Ventricle. *Circulation Research*, Vol. 35, No. 1, 1974, pp. 117-126

Thoennissen, N.; Allroggen, A.; Ritter, M.; Dittrich, R.; Schmid, C.; Schmid, H.; Ringelstein, E. & Nabavi, D.G. (2006). Influence of Inflammation and Pump Dynamic on Cerebral Microembolization in Patients with Continuous-Flow DeBakey LVAD. *American Society of Internal Artificial Organs (ASAIO)* , Vol. 52, No. 3, pp.243-247

Vollkron, M.; Schima, H.; Huber, L.; Benkowski, R.; Morello, G. & Wieselthaler, G. (2004). Development of a Suction Detection System for Axial Blood Pumps. *Artificial Organs*, Vol. 28, No. 8, 2004, pp. 709-716

Vollkron, M.; Schima, H.; Huber, L.; Benkowski, R.; Morello, G. & Wieselthaler, G. (2006). Advanced Suction Detection for an Axial Flow Pump. *Artificial Organs*, Vol. 30, No. 9, 2006, pp. 665-670

Wang, Y.; Faragallah, G.; Divo, E. & Simaan, M. (2011). Detection of Ventricular Suction in an Implantable Rotary Blood Pump Using Support Vector Machines. *Proceedings of the 33rd IEEE Annual International Conference of Engineering in Medicine and Biology*, Boston, MA, 2011

Yu, Y-C.; Boston, J.; Simaan, M. & Antaki, J. (1998). Estimation of Systemic Vascular Bed Parameters for Artificial Heart Control. *IEEE Transactions on Automatic Control*, Vol. 43, No. 6, 1998, pp. 765-778

Yuhki, A.; Hatoh, E.; Nogawa, M.; Miura, M.; Shimazaki, Y. & Takatani, S. (1999). Detection of Suction and Regurgitation of the Implantable Centrifugal Pump Based on the Motor Current Waveform Analysis and its Application to Optimization of the Pump Flow. *Artificial Organs*, 1999, Vol. 23, pp. 532-537
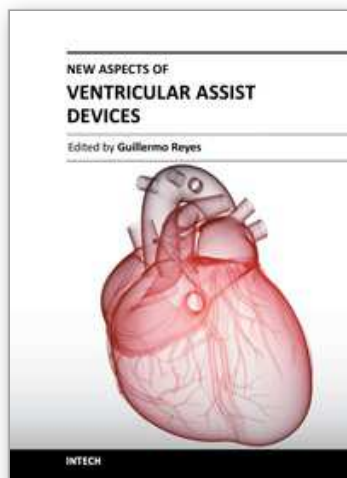
New Aspects of Ventricular Assist Devices

Edited by Dr. Guillermo Reyes

Ventricular assist device has become one of the standard therapies for the support and the management of the failing heart. Updating our knowledge about these devices is mandatory in order to improve patient outcomes. In this book we can read the efforts made by many physicians concerned with the treatment of heart failure with mechanical devices. We all hope that the information compiled by experts in ventricle assist devices in this book will help us all to do better our main task - heal patients.

How to reference

In order to correctly reference this scholarly work, feel free to copy and paste the following:

Marwan A. Simaan, George Faragallah, Yu Wang and Eduardo Divo (2011). Left Ventricular Assist Devices: Engineering Design Considerations, New Aspects of Ventricular Assist Devices, Dr. Guillermo Reyes (Ed.), ISBN: 978-953-307-676-8, InTech, Available from: http://www.intechopen.com/books/new-aspects-of-ventricular-assist-devices/left-ventricular-assist-devices-engineering-design-considerations

INTECH
open science | open minds